Mechanisms in non-heme iron oxidation catalysis

Chen, Juan

CHAPTER 4

Selective Photo-Induced Oxidation with O_2 of a Non-Heme Iron(III) Complex to a Bis(imine-pyridyl)iron (II) Complex

Non-heme iron(II) complexes of pentadentate N4Py (*N,N*-bis(2-pyridylmethyl)-*N*-bis(2-pyridyl)methylamine) type ligands undergo visible light-driven oxidation to their iron(III) state in the presence of O_2 without ligand degradation. Under mildly basic conditions, however, highly selective base catalyzed ligand degradation with O_2, to form a well-defined pyridyl-imine iron(II) complex and an iron(III) picolinate complex, is accelerated photochemically. Specifically, a pyridyl-CH_2 moiety is lost from the ligand, yielding a potentially N4 coordinating ligand containing an imine motif. The involvement of reactive oxygen species other than O_2 is excluded; instead, deprotonation at the benzylic positions to generate an amine radical is proposed as the rate determining step. The selective nature of the transformation holds implications for efforts to increase catalyst robustness through ligand design.

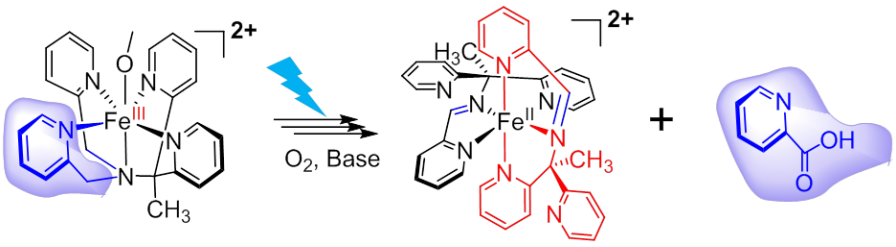

This chapter has been published:

Juan Chen, Duenpen Unjaroen, Stepan Stepanovic, Annie van Dam, Maja Gruden, Wesley R. Browne, *Inorganic chemistry, DOI 10.1021/acs.inorgchem.8b00187*

4.1 Introduction

The switch to catalysis employing sustainable and earth-abundant metals, in particular first row transition metals, such as manganese, copper, and iron, continues to be a major challenge. Non-heme iron complexes have received substantial attention in the catalyzed oxidation of organic substrates, in particular those complexes based on the pyridyl-alkylamine type ligands that are inspired by structural and mechanistic studies of the active sites of metallo-enzymes.[1] Typical examples of such ligands are the amine-based N4 and N5 ligands (e.g., TMC, 1,4,8,11-tetramethyl-1,4,8,11-tetraazacyclotetradecane;[2] TPA, tris(2-pyridylmethyl)amine;[3] and N4Py, N,N-bis(2-pyridylmethyl)-N-bis(2-pyridyl)methylamine,[4] as well as their derivatives) which have been used to isolate especially iron(IV) oxido species and establish their relevance in oxidation catalysis.[3–8] For many of these catalysts, deactivation due to ligand degradation is a major challenge to their broader application.[9–11] The presence of reactive oxidation species is intrinsic to oxidation reactions. Hence, building more robust catalyst systems requires intimate knowledge of ligand degradation mechanisms. Furthermore, the rapidly increasing interest in photocatalytic reactions, e.g., with iron complexes,[12,13] adds an extra dimension to understanding ligand degradation and catalyst deactivation.

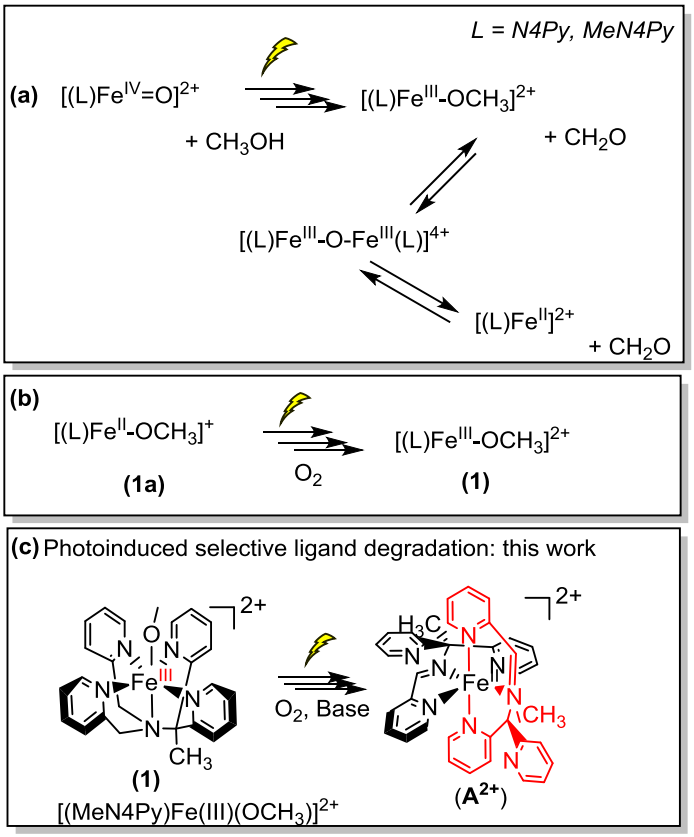

Scheme 7. Light-driven (a) reduction of Fe(IV)=O[14] and Fe(III)-O-Fe(III) with methanol oxidation,[15] (b) oxidation of Fe(II) complexes with O_2[16] and (c) light induced oxidative selective ligand degradation described here.

Recently we reported the photochemistry of a group of complexes based on pentadentate ligands (*e.g.*, N4py and MeN4py (L)), in their Fe(II),[16] Fe(III), and Fe(IV) oxidation states (**Scheme 7**).[14] Visible irradiation of **1a** {Fe(II)L(OCH_3)} in air-equilibrated methanol results in its oxidation to **1** (Fe(III)L(OCH_3), **Scheme 7**b), which could be reversed quantitatively by electrochemical or

chemical reduction. More recently we demonstrated that the Fe(IV)=O and Fe(III)-O-Fe(III) complexes of MeN4Py and N4Py undergo reduction to $[(MeN4Py)Fe^{III}(OCH_3)]^{2+}$ (**1**) and $[(MeN4Py)Fe^{II}(OCH_3)]^{+}$ (**1a**), respectively, upon near-UV irradiation in the absence of oxygen (with concomitant oxidation of methanol to methanal, **Scheme 7**a). In these studies, although the photo-induced oxidations and reductions proceeded without ligand degradation, it was noted that irreversible changes occurred under extended irradiation (several hours), in the presence of O_2, to yield an unassigned species.

Here we show under basic conditions an additional light induced pathway (**Scheme 7**c) that leads to selective oxidative ligand degradation that occurs in the presence of O_2 and a base. Specifically, a pyridyl-CH_2 moiety is lost from the MeN4Py ligand, yielding a potentially N4 coordinating ligand containing an imine motif. The degraded ligand then coordinates to the Fe(II) ion in a 2:1 manner to form $\mathbf{A^{2+}}$. The remaining iron ions form Fe(III) complexes of picolinate. $\mathbf{A^{2+}}$ is photochemically inert, and its formation is shown to be driven by an initial deprotonation followed by reaction with O_2 rather than C-H oxidation by an Fe(IV)=O intermediate or other reactive oxygen species. The mechanism for the formation of the photoproduct is explored, and the implications this light-driven reaction holds for ligand design strategies to avoid ligand breakdown in oxidation catalysis are discussed.

The selectivity observed in the case of the MeN4Py complex contrasts with that observed for the corresponding N4Py complex, which forms an ill-defined mixture of species. The highly selective nature of the conversion of **1** to $\mathbf{A^{2+}}$, in the case of the MeN4Py complex, allows for quantitative conversion to a complex bearing two singly oxidized MeN4Py ligands, which were isolated and characterized by UV-vis absorption, (resonance) Raman spectroscopy, FTIR and variable temperature ^{1}H NMR spectroscopy, ESI-MS analysis, cyclic voltammetry, and UV-vis absorption spectroelectrochemistry. ^{1}H NMR spectral and DFT data reveal that $\mathbf{A^{2+}}$ is a mixture of several relatively rapidly interconverting isomers of the complex.

4.2 Results and Discussion

The UV-vis absorption spectrum of **1** in methanol with Et_3N shows the appearance of new bands at 575 nm over time (i.e., 10 h, **Figure 63**). Irradiation (λ_{exc} = 365 nm) accelerates (< 5 min) the appearance of the 575 nm band, as well as bands at 380 and 492 nm dramatically (**Figure 63**). Similar changes are observed with NaOAc instead of Et_3N (**Figure 64**). The wavelength dependence of the rate of formation of $\mathbf{A^{2+}}$ corresponds to the absorbance with irradiation at 300, 405, and 457 nm showing rapid conversion. Irradiation at 590 nm results in an increase in absorbance at 575 nm at a much slower rate but, nevertheless, a rate greater than that observed for the thermal reaction alone (**Figure 65**).

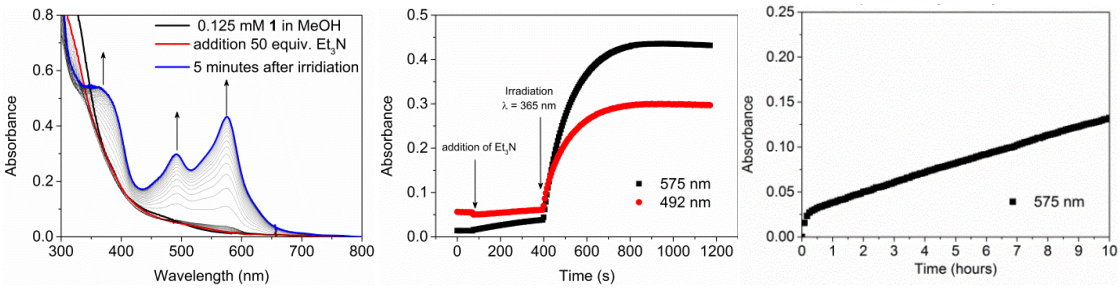

Figure 63. (left) UV-vis absorption spectra of **1** (0.125 mM) (black) in methanol under irradiation at 365 nm with 50 equiv Et_3N. (middle) Absorbance at 492 and 575 nm; Et_3N was added at 75 s, and

irradiation initiated at 400 s. (right) Absorbance of **1** (0.125 mM) in methanol with 50 equiv Et_3N at 575 nm over time (without irradiation - a JASCO V-570 UV-vis-NIR spectrometer at a single wavelength was employed to avoid photochemically induced changes).

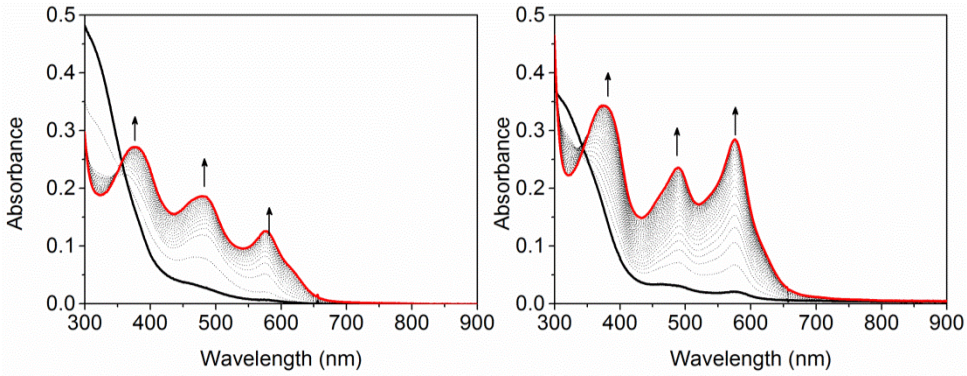

Figure 64. UV-vis spectrum of **1** in air-equilibrated methanol before (black) and during irradiation (λ_{exc} = 365 nm) (dotted lines)with the final spectrum in red: with presence of 50 equiv (left) and 250 equiv (right) of NaOAc.

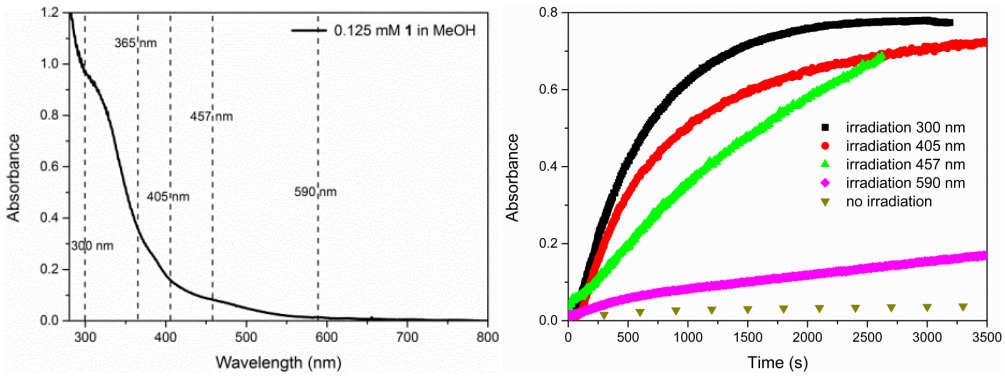

Figure 65. (left) Correspondence of irradiation wavelengths used with the UV-vis absorption spectrum of **1** in methanol and (right) absorbance at 575 nm over time showing the photochemical conversion of **1** to $\mathbf{A^{2+}}$ with 50 equiv Et_3N (irradiation commenced 5 min after addition of Et_3N in each case).

The presence of a base and O_2 is sufficient for achieving the conversion of **1** to $\mathbf{A^{2+}}$, albeit over several hours (**Figure 63**), indicating that light accelerates an otherwise thermal reaction. In the absence of added base (i.e., Et_3N, NaOAc, etc.), the formation of $\mathbf{A^{2+}}$ is not significant. Furthermore, irradiation of **1** in deoxygenated methanol results in its photoreduction to $[(MeN4Py)Fe^{II}OCH_3]^{2+}$ (**1a**) only, even in the presence of a base (**Figure 66** and **Figure 67**) (equation 1b), confirming that O_2 is essential in the formation of $\mathbf{A^{2+}}$. In the presence of a base and O_2, reduction to **1a** competes with the formation of $\mathbf{A^{2+}}$ (equation 1a and equation 1b) and the product ratio (**1a** vs $\mathbf{A^{2+}}$) is dependent on the time delay between addition of the base and commencement of irradiation (**Figure 68**).

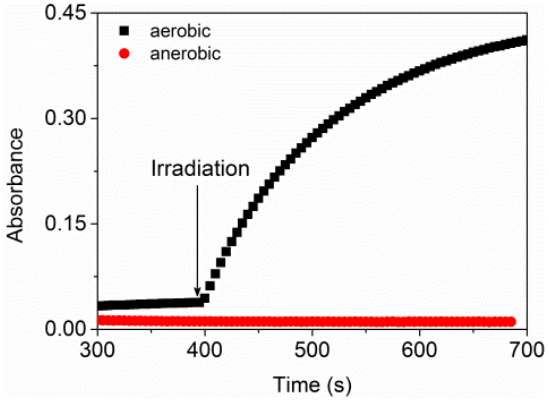

Figure 66. Absorbance at 575 nm of **1** in argon purged (red) and air-equilibrated (black) methanol over time. Irradiation was initiated 400 s after addition of 50 equiv of Et_3N. See **Figure 63** and **Figure 67** for full spectra.

$$\mathbf{1} \xrightarrow[\text{methanol}]{h\nu,\ \text{base},\ O_2} \mathbf{A^{2+}} \qquad \text{(a)}$$

$$\mathbf{1} \xrightarrow[\text{methanol}]{h\nu,\ \text{base},} \mathbf{1a} \qquad \text{(b)}$$

Indeed almost full conversion from **1** to $\mathbf{A^{2+}}$ was observed where irradiation was commenced 3-5 min after addition of base to **1** in methanol, with the quantum yield at 365 nm of ca. 0.14, whereas if irradiation is commence immediately after addition of the base, a mixture of $\mathbf{A^{2+}}$ and **1a** is obtained (**Figure 68**). Furthermore, whereas[5] addition of excess (50 equiv) H_2O_2 to **1** and anaerobic photo-product **1a**[15] leads to immediate formation of a Fe(III)-OOH species, while addition of H_2O_2 to $\mathbf{A^{2+}}$ has no effect on its absorption spectrum (**Figure 69**), which is contrast with the parent complex.

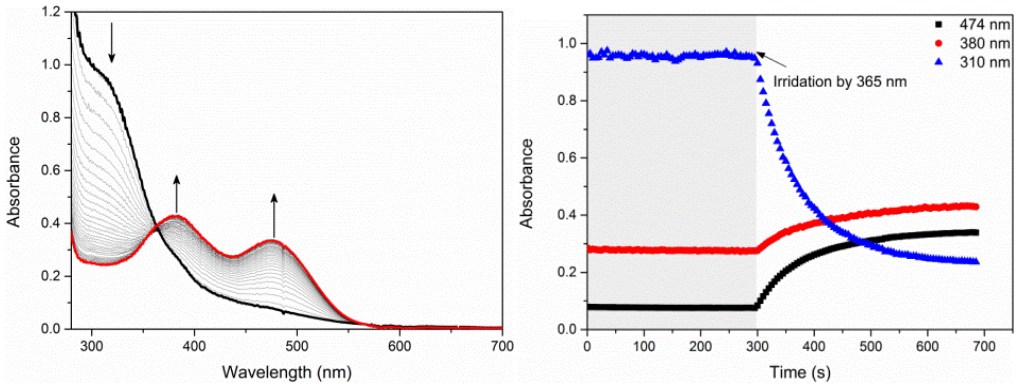

Figure 67. (Left) UV-vis absorption spectrum of **1** (0.125 mM, black) with 50 equiv Et_3N in argon purged methanol and under irradiation at 365 nm. Final spectrum shown in red. (Right) Absorbance at 474, 380 and 310 nm, before and during irradiation at 365 nm.

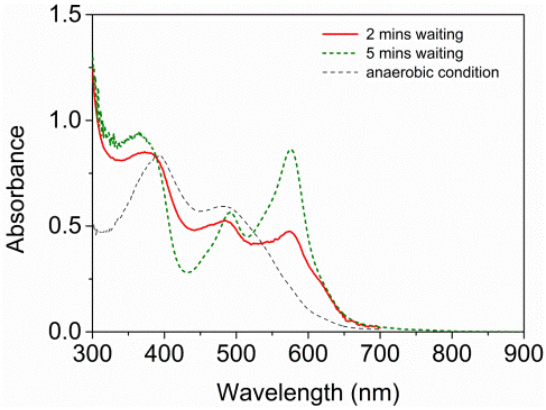

Figure 68. UV-vis spectra of the reaction mixture of **1** (0.25 mM) in methanol with 50 equiv Et_3N after irradiation (λ = 365 nm): (red solid line) irradiation commenced 2 minutes after addition of Et_3N, (green dash line) irradiation commenced 5 minutes after addition of Et_3N, (grey dash line) irradiation commenced immediately after addition of Et_3N.

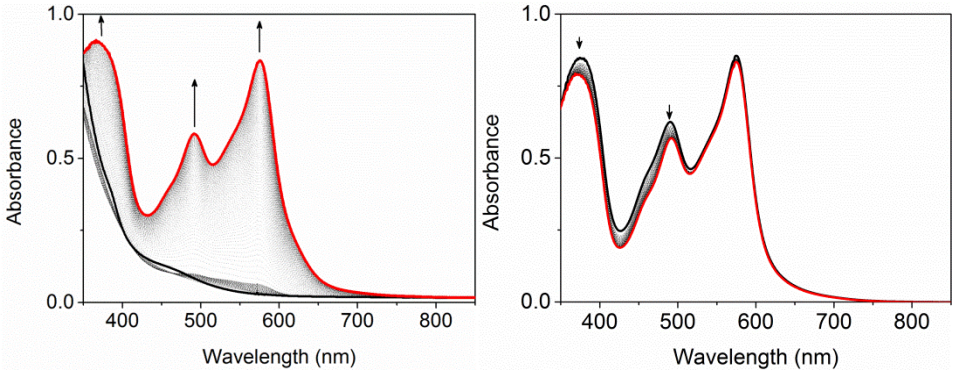

Figure 69. (left) UV-vis spectrum of **1** (0.25 mM) in methanol with 50 equiv Et_3N during irradiation (λ_{exc} = 365 nm, irradiation commenced 5 minutes after addition of Et_3N), (right) addition of 50 equiv H_2O_2 to the solution after irradiation (the minor decrease at 380 and 490 nm due to reaction of H_2O_2 with residual $[(MeN4Py)Fe^{II}OCH_3]^{2+}$ formed in competition with formation of $\mathbf{A^{2+}}$).

The isolated photoproduct $\mathbf{A^{2+}}$ shows five absorption bands at 250, 285, 380, 492, and 575 nm in methanol (**Figure 70** and **Figure 71** (left)) and shows a quasi-reversible oxidation at 0.95 V vs Ag/AgCl (**Figure 70**). The full chemical reversibility of the oxidation was confirmed by UV-vis absorption spectroelectrochemistry with a full loss and recovery of visible absorbance with each cycle between 0.0 and 1.2 V. The visible absorption bands are similar to those reported[17,18] for the iron(II) complex of a bis-tridentate bidentate imine-based iron(II) complex ($\mathbf{B^{2+}}$, **Scheme 8**) and are distinct from that of $[(MeN4Py)Fe^{II}\text{-}OCH_3]$.[19] The spectrum is identical in methanol and in acetonitrile indicating solvent is not coordinated in $\mathbf{A^{2+}}$. $\mathbf{A^{2+}}$ shows no signals in its EPR (X-band) spectrum at 77 K (**Figure 71** (right)) and shows a ^{1}H NMR spectrum (*vide infra*) that is consistent with the assignment of $\mathbf{A^{2+}}$ as a low-spin (diamagnetic) mononuclear Fe(II) complex.

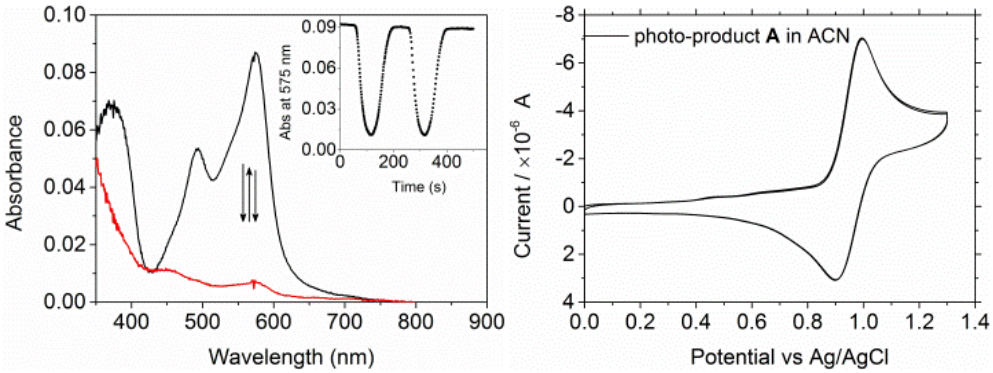

Figure 70. (left) UV-vis absorption spectrum of A^{2+} before and after oxidation at 1.2 V (inset: absorbance at 575 nm during cyclic voltammetry in an OTTLE cell). (right) Corresponding cyclic voltammetry of A^{2+} in acetonitrile (0.1 M $TBAPF_6$).

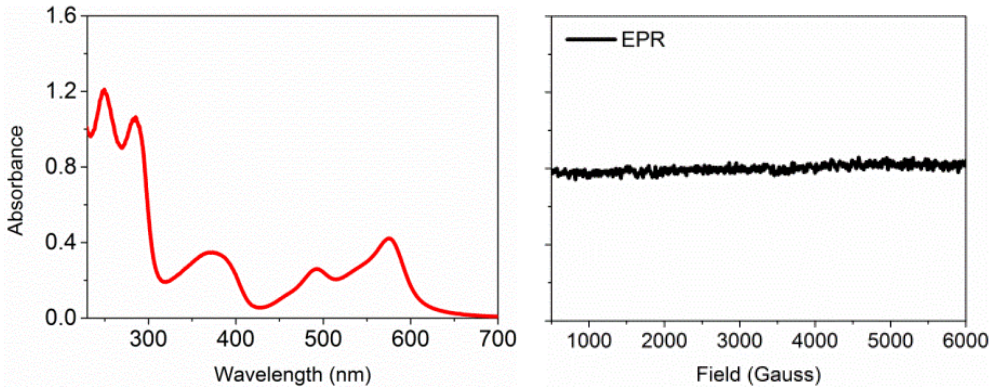

Figure 71. (left) UV-vis absorption spectrum of photo-product A^{2+} in methanol, (right) X-band EPR spectrum at 77 K of A^{2+} in methanol.

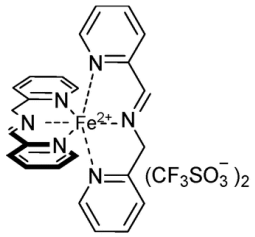

Scheme 8. Bis-tridentate imine-based iron(II) complex (B^{2+}-OTf) reported by Stefano and co-workers.[18]

The positive mode ESI/MS spectra of A^{2+} in methanol and acetonitrile show the same base peak at 316.3 m/z and a singly charged peak at 731.4 m/z corresponding to A^{2+} and $[A(ClO_4)]^+$, respectively. The observed ions are consistent with the complex $[L_2Fe(II)]^{2+}$ in which **L** is the MeN4Py ligand which has undergone a loss of one 'pyridine-CH_2 ' moiety. This assignment is consistent with the spectral similarity of complex A^{2+} and the pyridyl-imine-based complexes (**Scheme 8** and **Figure 72**) reported by Stefano and co-workers.[17,18]

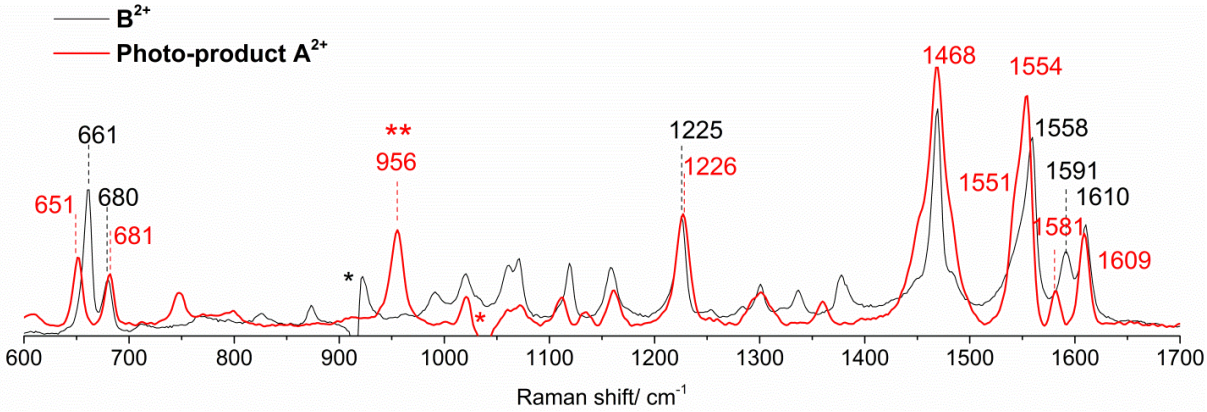

Figure 72. Resonance Raman spectra (λ_{exc} = 561 nm) of photo-product A^{2+} in methanol (red) with B^{2+} in acetonitrile (black). (*) artifacts due to imperfect solvent subtraction, (**) is ClO_4^-.

The presence of an imine bond in the ligand was confirmed by comparison of the non-resonant Raman and FTIR spectra of A^{2+} with those of $[(MeN4Py)Fe^{II}(CH_3CN)]^{2+}$ (**3**). The Raman spectrum of photoproduct A^{2+} in the solid state shows substantially modified ligand-based vibrational modes (1200 - 1600 cm^{-1}) compared to those of **3**. The band at 2270 cm^{-1}, a coordinated acetonitrile, is absent, and several intense bands at 1221, 1468, 1551 cm^{-1} appear in the spectrum of A^{2+} that are absent in the spectrum of **3** (**Figure 73**). The FTIR spectrum of A^{2+} reveals the presence of the same counterion as that in **3** (perchlorate $\nu_{stretch}$ (s) = 1087 cm^{-1}), as well as additional bands at 1217, 1245, 1353, 1542, and 1582 cm^{-1}.

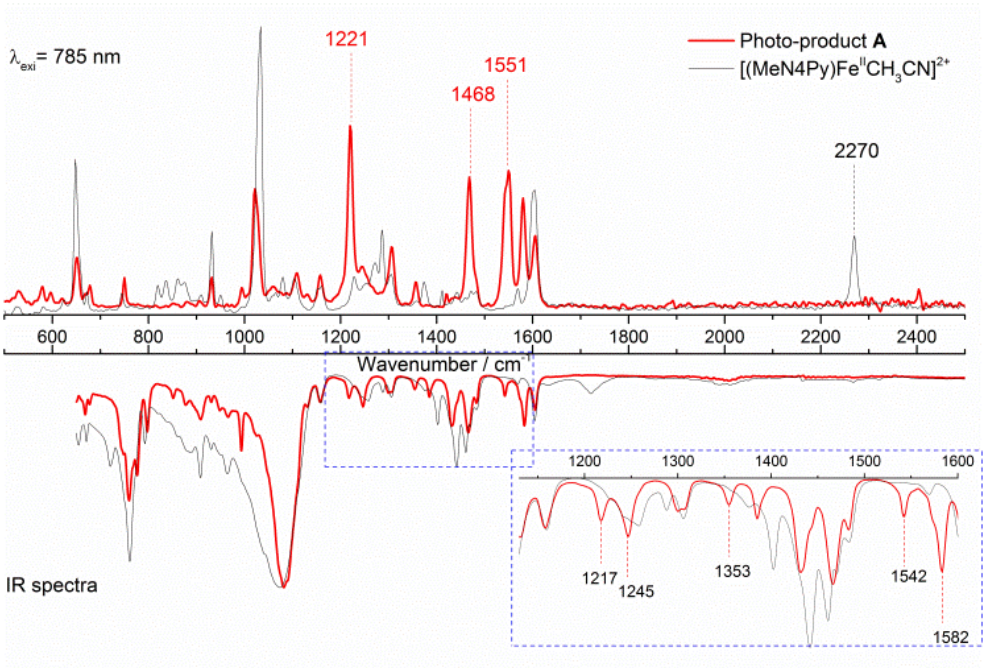

Figure 73. Raman (top) and FTIR (bottom) spectra of photoproduct A^{2+}, that are compared with those of complex $[(MeN4Py)Fe^{II}CH_3CN](ClO_4)_2$ (**3**). Inset: expansion of the region between 1130 and 1600 cm^{-1}.

The formation of the 2:1 (ligand : metal) complex of A^{2+} implies that 50% of the iron is present as a second complex. Furthermore, the pyridyl-CH_2 moiety lost in the formation of **L** should be accounted for. FTIR analysis for the light yellow precipitate formed during the conversion of **1** to A^{2+} shows strong bands at 841, 1284, and 1616 cm^{-1}. The spectrum resembles those of iron(III)

bis-picolinates, such as $[Fe^{III}_2(\mu\text{-}OMe)_2(Pic)_4]$ (PicH = 2-picolinic acid) which is formed upon mixing iron(III) salts and picolinic acid in methanol, but with minor differences in band positions (of the carboxylato modes, **Figure 74**)[20] and is consistent with the absence of significant ESI/MS peaks (as the complex is neutral) and EPR (X-band) signals at 77 K.

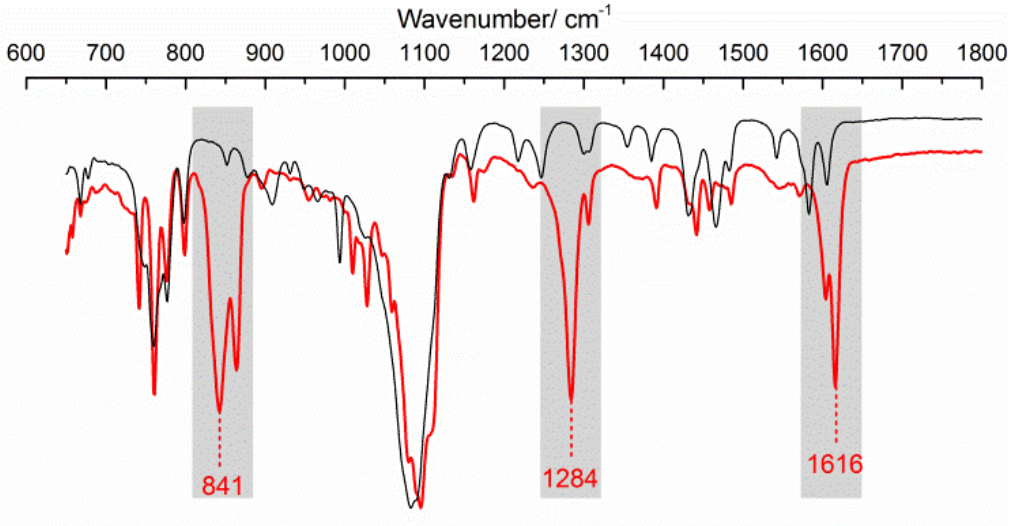

Figure 74. FTIR spectra of the obtained precipitates during the photochemical oxidation of **1** to $\mathbf{A^{2+}}$ (red) and photo-product $\mathbf{A^{2+}}$ (black).

The ^{1}H NMR spectrum of $\mathbf{A^{2+}}$ in acetonitrile-d_3 shows signals of a diamagnetic species that has a pronounced temperature dependent (**Figure 75**). At -30 °C, the spectrum indicates the presence of several species (isomers). At higher temperatures, rapid interconversion (with respect to the ^{1}H NMR time scale) is observed, leading to a substantial simplification of the spectrum. Two-dimensional (2D) NMR experiments (HSQC, HMBC, COSY, and NOESY) were conducted at -30 °C and at 75 °C to gain insight into the conformational chemistry and isomerization of $\mathbf{A^{2+}}$. At 75 °C, only one set of signals, consistent with C_2 symmetry, was observed. The signals at 10.76 and 2.39 ppm are assigned to imine and methyl protons, respectively (see supporting information in online paper, DOI: *10.1021/acs.inorgchem.8b00187*).[22] Twelve pyridyl signals are expected in the aromatic region; however, two are absent, due to extensive broadening. At 25 °C two sets of signals of distinct conformers are observed, which confirms that the exchange between isomers is slow with respect to ^{1}H NMR time scale. At -30 °C, the integration is consistent with the presence of four sets of signals, each of which has C_2 symmetry. Two sets of four singlet signals at δ 10.85, 10.82, 10.44, and 10.40 ppm (with a ratio of 1:1.2:0.8:1) and 2.95, 2.91, 2.88 and 2.84 ppm (with a ratio of 0.8:1:1:1.2) are assigned to imine and methyl protons, respectively.[22] The 2D NOESY NMR spectra confirm exchange among the four conformers affecting the imine, methyl, and several of the pyridine protons (see supporting information in online paper, DOI: *10.1021/acs.inorgchem.8b00187* for all 2D NMR spectra). The exchange pathways are proposed in **Figure 76**.

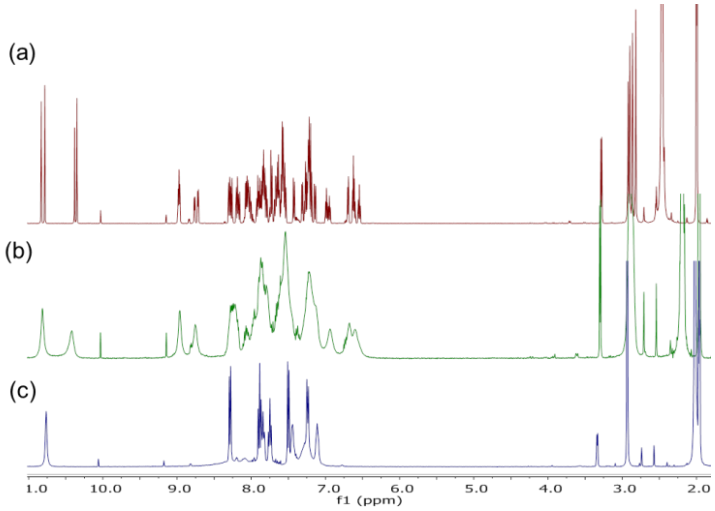

Figure 75. ^{1}H NMR spectra of photoproduct $\mathbf{A^{2+}}$ in CD_3CN at (a) -30 °C, (b) 25 °C, (c) 75 °C.

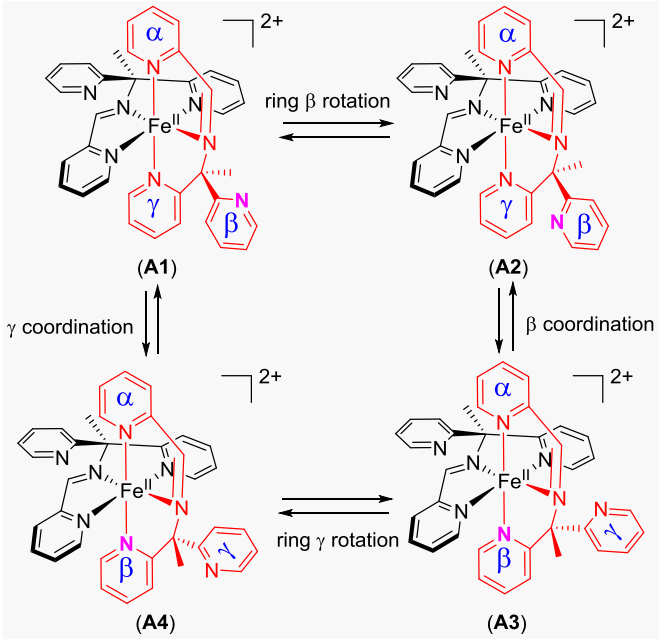

Figure 76. Proposed exchange pathways for $\mathbf{A^{2+}}$ in acetonitrile.

On the basis of the experimental data, the proposed structure of $\mathbf{A^{2+}}$ was explored with density functional theory (DFT) at the S12g level of theory; in particular, the relative stabilities, geometries, and electronic structure of conformers and diastereoisomers of the proposed bidentate imine-based Fe(II) complex $\mathbf{A^{2+}}$.were calculated. Stereochemical consideration of the complex $\mathbf{A^{2+}}$ must take into account the two stereogenic centers and, hence, there are seven distinct isomers (diastereoisomers and conformers, **Figure 77**). DFT calculations reveal that four lowest-energy isomers are similar in energy (**Table 5**) and that is reasonable to assume that the macroscopic properties are manifestations of the properties of a mixture of isomers and not a single thermodynamically stable isomer. Separate optimization of the three possible spin states (low, intermediate, and high) indicate clearly that the low-spin S=0 spin state is in all cases the spin ground state, with the other spin states around 20 kcal·mol^{-1} higher in energy (**Table 6**), consistent with the fully diamagnetic character of the species, cf. ^{1}H NMR spectroscopy, and confirming that the temperature dependence is due to isomer interconversion and not paramagnetism.

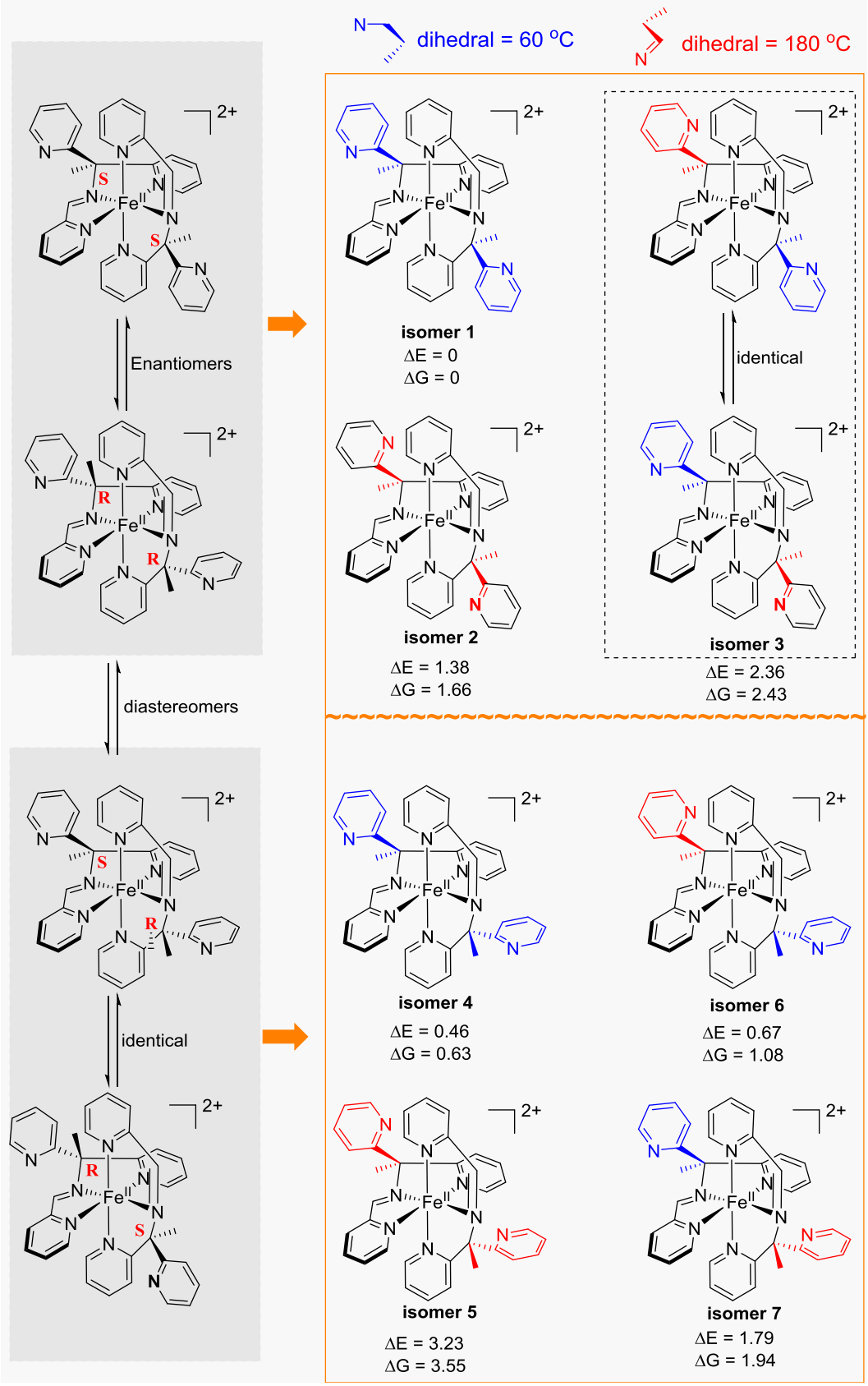

Figure 77. Schematically representation the origin of 7 different isomers of A^{2+}.

Table 5. Relative energies of 7 isomers of A^{2+} (kcal mol^{-1})

Structure	Electronic energy	Gibbs free energy
Isomer 1	0	0
Isomer 2	1.38	1.66
Isomer 3	2.36	2.43
Isomer 4	0.46	0.63
Isomer 5	3.23	3.55
Isomer 6	0.67	1.08
Isomer 7	1.79	1.94

Table 6. Relative spin state energies of 7 isomers of A^{2+} (kcal mol^{-1})

Structure	LS	IS	HS
Isomer 1	0	21.86	22.65
Isomer 2	0	18.98	19.03
Isomer 3	0	20.07	19.98
Isomer 4	0	21.46	22.10
Isomer 5	0	18.21	17.75
Isomer 6	0	19.81	22.11
Isomer 7	0	20.00	20.12

Although both O_2 and a base are required for the formation of A^{2+}, the mechanism by which the ligand is oxidized to lose a pyridyl-CH_2 moiety and form an imine is less apparent. The requirement for O_2 to be present implies the formation of a reactive oxygen species, such as Fe(IV)=O, hydroxyl radicals, superoxides, singlet oxygen etc., that can engage in hydrogen atom abstraction (HAT) at the benzylic C-H of the MeN4Py ligand. However, the involvement of singlet oxygen and superoxide can be excluded as neither results in the formation of photoproduct A^{2+} (see supporting information in online paper, DOI: *10.1021/acs.inorgchem.8b00187*). Furthermore, the Fe(II) complex bearing the same ligand **1a** is not converted directly to A^{2+} (see **Figure 78** and **Scheme 9**). Irradiation of the structurally analogous (N4Py) complex $[(N4Py)Fe(III)\text{-}OCH_3]^{2+}$ (**2**) in air-equilibrated methanol with Et_3N results in a mixture of Fe(II) complexes with an intact ligand (< 20%) and ill-defined ligand degradation products; no similar imine-based ligand complex "A^{2+}" was observed (**Figure 79**).

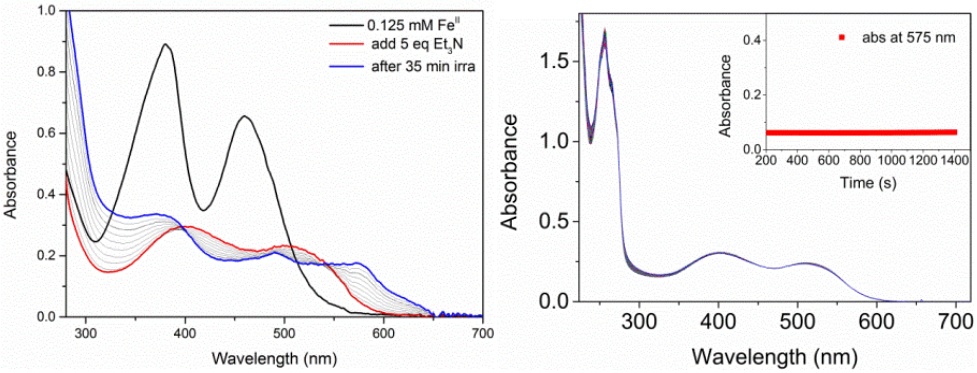

Figure 78. UV-vis absorption spectra of **1a** under irradiation (λ = 365 nm) in air-equilibrated (left) and deoxygenated (right) methanol in presence of Et_3N. Inset in right is corresponding absorbance at 575 nm over time.

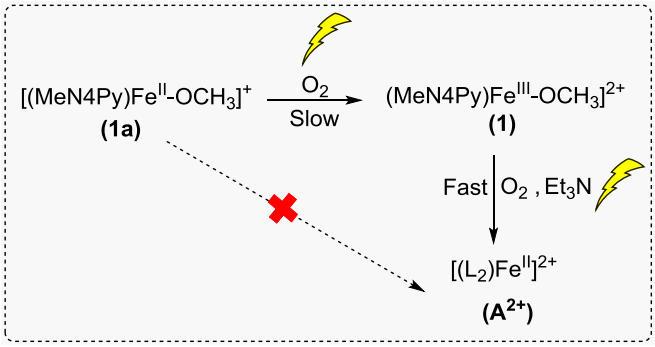

Scheme 9. Mechanism for formation of photo-product A^{2+} by irradiation of **1a** in air equilibrated methanol in presence of Et_3N.

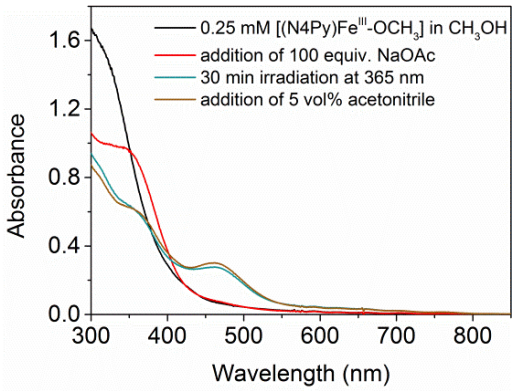

Figure 79. UV-vis absorption spectra of $[(N4Py)Fe^{III}\text{-}OCH_3]^{2+}$ (**2**) in methanol under irradiation in presence of 100 equiv NaOAc. (The amount of corresponding $[(N4Py)Fe^{II}(CH_3CN)]^{2+}$ was calculated by the absorbance coefficient ε_{458nm} = 6520 M^{-1} cm^{-1}).

Amine-based ligands are typically good donor ligands, and under irradiation ligand to metal charge transfer from the amine moiety to an iron(III) center is expected, yielding a transient aminium radical cation. The charge transfer lowers the bond dissociation energy of the C–H bonds at the amine α-position[23] and facilitates deprotonation and charge transfer to form a radical at the first methylene position. Such species are known to couple readily with O_2 to form an alkyl superoxide radical.[24] Hydrogen atom abstraction (HAT) from a neighboring methylene position induces C-N bond cleavage and finally formation of an imine. O_2 plays an important role in this

mechanism; however, deprotonation is rate limiting, and irradiation serves to make the benzylic C-H bonds more acidic, accelerating the overall process (Scheme 10).

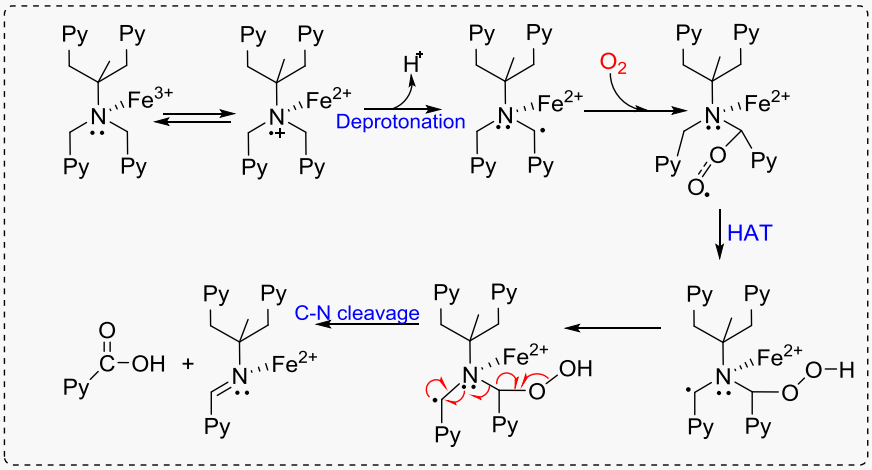

Scheme 10. Proposed mechanism for photoreduction and degradation of **1**.

Oxidative cleavage of a C-N bond was reported for the cobalt(II) complex of *N*-methyl-*N*,*N'*-bis(2-pyridylmethyl)ethylenediamine-*N'*–acetate (mebpena-), in which Co(III)-superoxide intermediates were proposed to react with methylene units with HAT as an initial step toward C-N bond cleavage.[25] The first iron(III) assisted oxidative cleavage of a C-N bond was reported by Morgenstern-Badarau following a similar mechanism.[26] In both cases, the products of the oxidative C-N cleavage of the tertiary amine ligand were secondary amines. In the present study, to the best of our knowledge, this is the first example of oxidative cleavage of a C-N bond leading to the formation of an imine ligand.

4.3 Conclusions

In summary, we report the highly selective oxidative ligand degradation in a non-heme iron(III) complex to form a well-defined imine-based 2:1 iron(II) complex under basic conditions with O_2 as the terminal oxidant. The reaction is accelerated dramatically by irradiation with near-UV and visible light; however, for both thermally and photochemically driven reactions, the initial step is assigned to deprotonation to form an alkylamine radical that subsequently undergoes reaction with O_2 instead of the formation of other reactive oxygen species, such as superoxides, hydroxyl radicals, or H_2O_2. The ligand degradation pathway holds implications for the design of ligands for oxidation catalysts based on the pyridyl-methylamine motif, where degradation is expected to be due to attack of reactive oxygen species and high-valent iron oxido complexes on the ligand. Here, we show that base catalyzed pathways are important also and that the observations may help rationalize in part the increased efficiency of such catalysts under acid conditions.

4.4 Experimental section

1,1-di(pyridin-2-yl)-N,N-bis(pyridin-2-ylmethyl)ethan-1-amine (MeN4Py),[27] complexes $[(MeN4Py)Fe^{III}(OCH_3)](ClO_4)_2$[27] (**1**) and $[(MeN4Py)Fe^{II}(CH_3CN)](ClO_4)_2$[5] (**3**), $[(N4Py)Fe^{III}(OMe)](ClO_4)_2$ (**2**)[28] were prepared as reported previously. $[(MeN4Py)Fe^{II}(OCH_3)]^+$ (**1a**) was generated by dissolving $[(MeN4Py)Fe^{II}(CH_3CN)](ClO_4)_2$[27] (**3**) in methanol.[16] Commercially available chemicals were purchased from Sigma Aldrich without further purification. All solvents used for spectroscopy were of UVASOL (Merck) grade. $[(MeN4Py)Fe^{III}(Cl)](ClO_4)_2$ (**1-Cl**) was prepared by mixing equimolar amounts of $Fe^{III}Cl_3$ and the ligand (MeN4Py) in acetonitrile, followed by addition

of 10 equiv $NaClO_4$ in a minimum amount of acetonitrile. Vapour diffusion of diethyl ether into the solution at room temperature provided single crystals of $[(MeN4Py)Fe^{III}(Cl)](ClO_4)_2$.

4.5 Acknowledgements

We thank Dr. Duenpen Unjaroen for the help with 2D NMR studies, Dr. Stepan Stepanovic for DFT calculations, and Dr. Annie van Dam for mass spectra measurements. The European Research Council (ERC 279549 to W.R.B.), the Serbian Ministry of Science (OI172035 to M.G.), the Chinese Scholarship Council (CSC to J.C.), and the Netherlands Ministry of Education, Culture, and Science (Gravity program 024.001.035 to W.R.B.) are acknowledged for their financial support. This work was performed in the framework of COST Action CM1305 (STSM 38503 and 39551) "Explicit Control Over Spin-states in Technology and Biochemistry (ECOSTBio)".

4.6 References

(1) Oloo, W. N.; Que, L. *Acc. Chem. Res.* 2015, *48* (9), 2612–2621.

(2) Rohde, J.-U.; In, J.-H.; Lim, M. H.; Brennessel, W. W.; Bukowski, M. R.; Stubna, A.; Münck, E.; Nam, W.; Que, L. *Science* 2003, *299* (5609), 1037–1039.

(3) Lim, M. H.; Rohde, J.-U.; Stubna, A.; Bukowski, M. R.; Costas, M.; Ho, R. Y. N.; Münck, E.; Nam, W.; Que, L. *Proc. Natl. Acad. Sci.* 2003, *100* (7), 3665–3670.

(4) Kaizer, J.; Klinker, E. J.; Oh, N. Y.; Rohde, J.-U.; Song, W. J.; Stubna, A.; Kim, J.; Münck, E.; Nam, W.; Que, L. *J. Am. Chem. Soc.* 2004, *126* (2), 472–473.

(5) Roelfes, G.; Lubben, M.; Hage, R.; Que, Lawrence, J.; Feringa, B. L. *Chem. – A Eur. J.* 2000, *6* (12), 2152–2159.

(6) Sastri, C. V; Sook Seo, M.; Joo Park, M.; Mook Kim, K.; Nam, W. *Chem. Commun.* 2005, *2* (11), 1405–1407.

(7) England, J.; Guo, Y.; Farquhar, E. R.; Young, V. G.; Münck, E.; Que, L. *J. Am. Chem. Soc.* 2010, *132* (25), 8635–8644.

(8) Oh, N. Y.; Suh, Y.; Park, M. J.; Seo, M. S.; Kim, J.; Nam, W. *Angew. Chemie Int. Ed.* 2005, *44* (27), 4235–4239.

(9) Thibon, A.; Bartoli, J.-F.; Bourcier, S.; Banse, F. *Dalton Trans.* 2009, *0* (43), 9587–9594.

(10) England, J.; Davies, C. R.; Banaru, M.; White, A. J. P.; Britovseka, G. J. P. *Adv. Synth. Catal.* 2008, *350* (6), 883–897.

(11) Grau, M.; Kyriacou, A.; Cabedo Martinez, F.; de Wispelaere, I. M.; White, A. J. P.; Britovsek, G. J. P. *Dalton Trans.* 2014, *43* (45), 17108–17119.

(12) Company, A.; Sabenya, G.; González-Béjar, M.; Gómez, L.; Clémancey, M.; Blondin, G.; Jasniewski, A. J.; Puri, M.; Browne, W. R.; Latour, J.-M.; Que, L.; Costas, M.; Pérez-Prieto, J.; Lloret-Fillol, J. *J. Am. Chem. Soc.* 2014, *136* (12), 4624–4633.

(13) Kotani, H.; Suenobu, T.; Lee, Y.-M.; Nam, W.; Fukuzumi, S. *J. Am. Chem. Soc.* 2011, *133* (10), 3249–3251.

(14) Chen, J.; Draksharapu, A.; Harvey, E.; Rasheed, W.; Que, L.; Browne, W. R. *Chem. Commun.* 2017, *53* (91), 12357–12360.

(15) Chen, J.; Stepanovic, S.; Draksharapu, A.; Gruden, M.; Browne, W. R. *Angew. Chemie Int. Ed.* 2018, *57* (12), 3207–3211.

(16) Draksharapu, A.; Li, Q.; Roelfes, G.; Browne, W. R. *Dalton Trans.* 2012, *41* (42), 13180–13190.

(17) Olivo, G.; Nardi, M.; Vìdal, D.; Barbieri, A.; Lapi, A.; Gómez, L.; Lanzalunga, O.; Costas, M.;

Di Stefano, S. *Inorg. Chem.* 2015, *54* (21), 10141–10152.
(18) Olivo, G.; Arancio, G.; Mandolini, L.; Lanzalunga, O.; Di Stefano, S. *Catal. Sci. Technol.* 2014, *4* (9), 2900–2903.
(19) Draksharapu, A.; Li, Q.; Logtenberg, H.; van den Berg, T. A.; Meetsma, A.; Killeen, J. S.; Feringa, B. L.; Hage, R.; Roelfes, G.; Browne, W. R. *Inorg. Chem.* 2011, *51* (2), 900–913.
(20) Kalinowska, M.; Borawska, M.; Świsłocka, R.; Piekut, J.; Lewandowski, W. *J. Mol. Struct.* 2007, *834–836*, 419–425.
(21) Kiani, S.; Tapper, A.; Staples, R. J.; Stavropoulos, P. *J. Am. Chem. Soc.* 2000, *122* (31), 7503–7517.
(22) Chavez-Gil, T. E.; Yasaka, M.; Senokuchi, T.; Sumimoto, M.; Kurosaki, H.; Goto, M. *Chem. Commun.* 2001, *0* (22), 2388–2389.
(23) Dinnocenzo, J. P.; Banach, T. E. *J. Am. Chem. Soc.* 1989, *111* (23), 8646–8653.
(24) Anjana, S.; Donring, S.; Sanjib, P.; Varghese, B.; Murthy, N. N. *Dalton Trans.* 2017, *46* (33), 10830–10836.
(25) Vad, M. S.; Nielsen, A.; Lennartson, A.; Bond, A. D.; McGrady, J. E.; McKenzie, C. J. *Dalton Trans.* 2011, *0* (40), 10698–10707.
(26) Rodriguez, M.-C.; Lambert, F.; Morgenstern-Badarau, I.; Cesario, M.; Guilhem, J.; Keita, B.; Nadjo, L. *Inorg. Chem.* 1997, *36* (16), 3525–3531.
(27) Draksharapu, A.; Li, Q.; Logtenberg, H.; van den Berg, T. A.; Meetsma, A.; Killeen, J. S.; Feringa, B. L.; Hage, R.; Roelfes, G.; Browne, W. R. *Inorg. Chem.* 2011, *51* (2), 900–913.
(28) Roelfes, G.; Lubben, M.; Chen, K.; Ho, R. Y. N.; Meetsma, A.; Genseberger, S.; Hermant, R. M.; Hage, R.; Mandai, S. K.; Young Jr., V. G.; Zang, Y.; Kooijman, H.; Spek, A. L.; Que Jr., L.; Feringa, B. L. *Inorg. Chem.* 1999, *38* (8), 1929–1936.